Journal of ELECTRONIC MATERIALS, Vol. 48, No. 7, 2019
https://doi.org/10.1007/s11664-019-07169-8

Facile One-Pot Synthesis of $LiMnO_2$ Nanowire-Graphene Nanoplatelet Composites and Their Applications in Battery-Like Electrodes for High Performance Electrochemical Capacitors

TAO CHEN[1] and JOONHO BAE[1,2]

1.—Department of Nano-physics, Gachon University, Seongnam-si, Gyeonggi-do 461-701, Republic of Korea. 2.—e-mail: jnana2k@gmail.com

In this work, the well-dispersed $LiMnO_2$ nanowires of diameter 100 nm were successfully prepared via a simple one-pot hydrothermal method. The morphology of the nanowires during their growth was dependent on the reaction time. The $LiMnO_2$ nanowires were possibly formed by a nucleation and regrowth process. The $LiMnO_2$ nanowires-graphene nanoplatelets ($LiMnO_2$ nanowires-GNP) composite was then prepared by the direct milling of one-dimensional $LiMnO_2$ nanowires and two-dimensional GNP. The $LiMnO_2$ nanowires-GNP composite was employed as an electrode material to investigate its electrochemical performance. The $LiMnO_2$ nanowires-GNP composite exhibited an outstanding mass-specific capacitance of 147 F g^{-1} at 5 mV s^{-1}, as revealed by cyclic voltammetry measurement. This was more than three times higher than that exhibited by $LiMnO_2$ nanowires (41 F g^{-1}). The cycling performance of $LiMnO_2$ nanowires-GNP electrode revealed a capacitance retention of 86% after 1000 charge–discharge cycles at 5 A g^{-1}, which was superior to that exhibited by the $LiMnO_2$ nanowires. Besides, the resistance of the $LiMnO_2$ nanowires-GNP was lower than that of $LiMnO_2$ nanowires, demonstrating that these hybrids could be considered as next generation electrode materials for electrochemical energy storage and conversion devices.

Key words: $LiMnO_2$, nanowires, electrochemical capacitors

INTRODUCTION

Over the past few years, significant efforts have been devoted to the development of alternative energy storage and conversion devices of high energy and power densities and long cycle time. This is primarily because of the gradually increasing environmental concerns and the exhausting fossil fuels.[1] It is extremely essential for researchers to explore various kinds of energy storage and conversion systems. Until now, as an intermediate system between dielectric capacitors and batteries, electrochemical capacitors have attracted much attention as next generation energy storage devices because of their high power density and good cycling performance.[2,3] However, their lower energy density as compared with that of the batteries restricts their application as next generation energy devices. An effective method of enhancing the energy density is to improve the capacitive performance of electrochemical capacitors.[4,5] The most effective strategy for optimizing the capacitive performance is to develop hybrid electrodes with carbon materials and metal oxides,[6–8] wherein the carbon materials serve as a physical support for metal oxides and provide efficient electron transfer channels to improve the power density and conductivity of the metal oxide materials. These metal oxide materials store the charge of redox reactions and render high energy density to these electrodes. These hybrid electrodes can overcome the individual defects of the carbon and metal oxide materials. Therefore, in

(Received October 19, 2018; accepted March 22, 2019; published online April 12, 2019)

order to achieve capacitors with outstanding electrochemical performance, it is essential to develop hybrid electrode materials possessing outstanding electrical conductivity and high charge storage capacity.

Nanowires and nanoplatelets can significantly influence the performance of supercapacitors, because the shorter distance in the low dimensional materials render high rates of metal ion transport during intercalation and deintercalation.[9–11] Although there are many reports on the synthesis of low dimensional materials, the preparation of one-dimensional cathode nanowires still proves to be a challenge.[12] $LiCoO_2$,[13] $LiFePO_4$,[14] $Na_{0.35}MnO_2$,[15] and $K_{0.19}MnO_2$[16] nanowires have been synthesized by a template-assisted method using porous SiO_2 template or MnO_2 nanowire template. However, as cathodes in supercapacitors, these composite metal oxide nanowires do show very high capacitance compared with the corresponding bulk materials. Recently, the introduction of carbon materials was found to be effective in enhancing the electrochemical properties of the composite metal oxide nanowires.[17] Particularly, layered graphene, owing to its large surface area, excellent conductivity, and chemical stability, was found to be an outstanding carbon substrate for hosting active materials in storage energy systems.[18] For example, Rai et al. prepared a novel hybrid material of $Ni(OH)_2$ and reduced graphene oxide by a facile non-hydrothermal route. This material had a high specific capacitance of 1671.7 F g^{-1} at a current density of 1 A g^{-1}.[19] Ultrafine NiO dot/graphene flakes synthesized using a green electrochemical alternating voltage method exhibited a specific capacitance of 1181.1 F g^{-1}, which was much higher than that exhibited by pure NiO dots.[20] Moreover, Wang et al. reported the synthesis of Co_3O_4 nanoclusters on flocculent graphene/nickel foam, which showed an improved specific capacitance of 1615 F g^{-1}, as compared with the capacitance of 968 F g^{-1} exhibited by Co_3O_4 on bare nickel foam.[21] The overall performance was enhanced because the large surface area and high electrical conductivity of the hybrid material favored a facile charge transport, while the layer structure ensured the easy diffusion of electrolytes.

In this work, uniform $LiMnO_2$ nanowires were successfully prepared via a one-pot hydrothermal method. We also employed $LiMnO_2$ nanowires-graphene nanoplatelets (GNP) composite as a hybrid electrode material in electrochemical capacitors. The hybrid electrode could overcome the defects of carbon materials and transition metal oxide materials. GNP served as a physical support for $LiMnO_2$ nanowires and provided an efficient electron transfer channel to increase the conductivity of $LiMnO_2$ nanowires, which could store the charge of redox reactions and impart high energy density to the electrodes. To the best of our knowledge, only a few studies on the synthesis of $LiMnO_2$ nanowires-GNP composite have been reported thus far. The electrochemical performances of the $LiMnO_2$ nanowires-GNP composite as well as the individual components were investigated for comparison. A possible formation mechanism of $LiMnO_2$ nanowires has also been proposed. The capacitance of $LiMnO_2$ nanowires-GNP composite in 1 M KOH electrolyte was much higher than that of the individual components. It exhibits superior charge–discharge properties and outstanding cycling lifetime, suggesting their potential application in energy storage systems.

EXPERIMENTAL SECTION

Synthesis of $LiMnO_2$ Nanowires

All the reagents were of analytical grade and used directly without further purification. Typically, 0.2 g of Mn_2O_3 powder was dispersed in 50 ml of 5 M aqueous LiOH. After stirring for 30 min, the above suspension was transferred into the Teflon-lined autoclave and heated at 205°C. Samples were withdrawn at intervals of 24 h, 48 h, 72 h, and 96 h for analyses. Subsequently, the wine brownish black precipitate was separated by centrifugation and washed several times with deionized water and ethanol before drying at 100°C in an oven. The final products were collected for characterizations and further preparation of $LiMnO_2$ nanowires-GNP composite.

Synthesis of $LiMnO_2$ Nanowires-GNP Composite

Commercial GNP was purchased from Plasmachem. Typically, 0.008 g GNP and 0.024 g $LiMnO_2$ nanowire powder were dispersed in 40 mL isopropyl alcohol, and the dispersion was exposed to ultrasound irradiation under ambient air for 120 min. The black mixture was centrifuged, and the precipitate was washed with deionized water and ethanol several times before drying at 80°C in an oven. The final products were obtained for characterization and further preparation of the electrode material.

Characterizations

The phases of the synthesized samples were examined by x-ray powder diffraction (XRD) using Cu Kα-radiation (λ = 0.154 nm) at a scanning rate of 5º min^{-1} in the 2θ range from 10° to 80°. The morphologies and sizes of the powders were examined by field emission scanning electron microscopy (FESEM; JSM-6360LA, Japan). N_2 adsorption–desorption isotherms were recorded on a Micromeritics ASAP 2010 adsorption analyzer, and the Brunauer–Emmett–Teller (BET) specific surface area was calculated.

The electrode materials were prepared by mixing powdered $LiMnO_2$ nanowires-GNP composite, activated carbon, and poly (vinyl alcohol) onto a nickel

foam, at a weight ratio of 80:10:10. KOH (1 M) was used as the electrolyte. $LiMnO_2$ nanowire electrode for the control experiment was prepared in a way similar to that of the $LiMnO_2$ nanowires-GNP composite electrode.

The electrochemical properties of the synthesized samples were measured in a three-electrode cell system, in which a saturated Ag-AgCl electrode (SCE) and Pt were used as the reference and counter electrodes, respectively. Cyclic voltammetry (CV) and galvanostatic charge–discharge curves were recorded on a Princeton Applied Research Electrochemical Workstation. The capacitance was calculated based on the weight of the active cathode material. The specific capacitance (C) is defined by the equation: $C = (\int I\mathrm{d}V)/(m * \Delta V * v)$, where I, m, v, and ΔV represent the working current, mass of active materials, scan rate of the working current, and range of voltage, respectively.

RESULTS AND DISCUSSION

The XRD pattern of the brown powdered sample prepared hydrothermally is displayed in Fig. 1. All the main diffraction peaks could be indexed to a spinel phase $LiMnO_2$ with lattice parameters a = 2.812 Å and c = 1.629 Å, which was consistent with the standard XRD database (PDF card No. 09-0109). No diffraction peaks corresponding to impurities were observed in the XRD pattern, indicating that the product was entirely composed of pure $LiMnO_2$ nanowires.

The SEM images of $LiMnO_2$ samples at various time points during its synthesis, keeping the other conditions constant, are shown in Fig. 2. Figure 2a shows that a small amount of nanoplatelets and some bulk precursor were obtained after 24 h in the one-pot hydrothermal synthesis. After for 48 h (Fig. 2b), two-dimensional layered products with large surface area were observed, which gradually grew into a one-dimensional assembly of nanowires along one growth direction of microplates after 72 h (Fig. 2c). After 96 h, well-dispersed and uniform $LiMnO_2$ nanowires (Fig. 2d) were obtained, along with a concomitant disappearance of the nanoplatelets. The nanowires were about 100 nm in diameter. The above results indicated that the morphology of $LiMnO_2$ nanowires was strongly influenced by the reaction time.

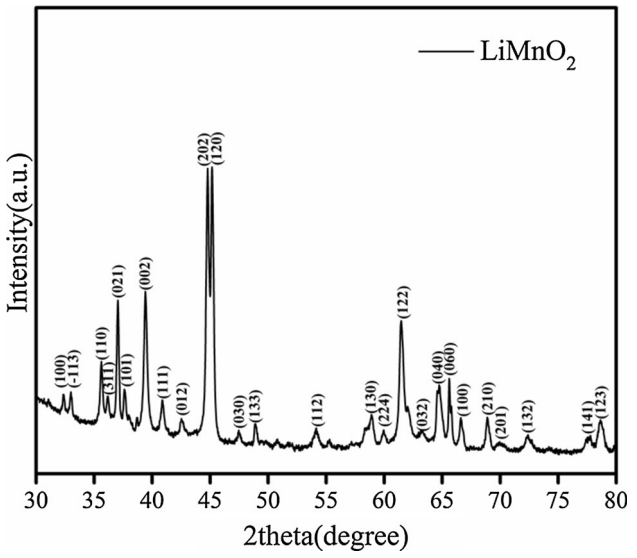

Fig. 1. XRD pattern of $LiMnO_2$ powders synthesized hydrothermally.

Based on the morphology transformation at different time points in the reaction, we speculated that the formation of $LiMnO_2$ nanowires followed the nucleation and regrowth process[22]; a possible formation mechanism of different morphologies is illustrated in Fig. 3. With increasing reaction time, the $LiMnO_2$ products gradually changed from nanoplatelets to nanowires, because the precursor Mn_2O_3 behaved as a thermodynamically stable nucleus onto which Mn_2O_3 could diffuse. This helped $LiMnO_2$ transform into nanowires. Moreover, the uniformity of the nanowires was better with prolonged reaction times, as the nanoplatelets disappeared, and the one-dimensional nanowires appeared.[23]

The typical XRD pattern and SEM image of $LiMnO_2$ nanowires-GNP composite (mass ratio of $LiMnO_2$ nanowires to GNP is 3:1) are shown in Fig. 4. Figure 4a shows that the $LiMnO_2$ nanowires-GNP composite displays two kinds of phases. The main phase comprised pure $LiMnO_2$ nanowires, which was consistent with the data in Fig. 1 (PDF card No. 19-0105). The diffraction peaks at 2θ values of 25° and 42.5° (labelled with triangles) are consistent with the GNP phase. No diffraction peaks corresponding to the impurities were observed in the XRD pattern, indicating that the product was composed of $LiMnO_2$ nanowires and GNP only. The SEM image at the right of Fig. 4b confirmed the successful fabrication of the $LiMnO_2$ nanowires-GNP composite, which was achieved by sonicating a mixture of one-dimensional $LiMnO_2$ nanowires and two-dimensional GNP for 1 h. The final products were collected for further electrochemical experiments.

The N_2 adsorption–desorption isotherms of $LiMnO_2$ nanowires and $LiMnO_2$ nanowires-GNP composite are displayed in Fig. 5. The figure in the inset shows their corresponding pore size distributions. For the $LiMnO_2$ nanowires-GNP composite, the BET surface area and pore volume are 73.9 $m^2\ g^{-1}$ and 0.15 $cm^3\ g^{-1}$, respectively, which are larger than those of the $LiMnO_2$ nanowires (4.1 $m^2\ g^{-1}$ and 0.014 $cm^3\ g^{-1}$).

The electrochemical performances of the samples as cathodes in an electrochemical capacitor were examined in a three-electrode system by using 1 M KOH as the electrolyte. The CV curves of the $LiMnO_2$ nanowires and $LiMnO_2$ nanowires-GNP composite, recorded at scan rates varying from 5 mV s^{-1} to 100 mV s^{-1}, are shown in Fig. 6a and b, respectively.

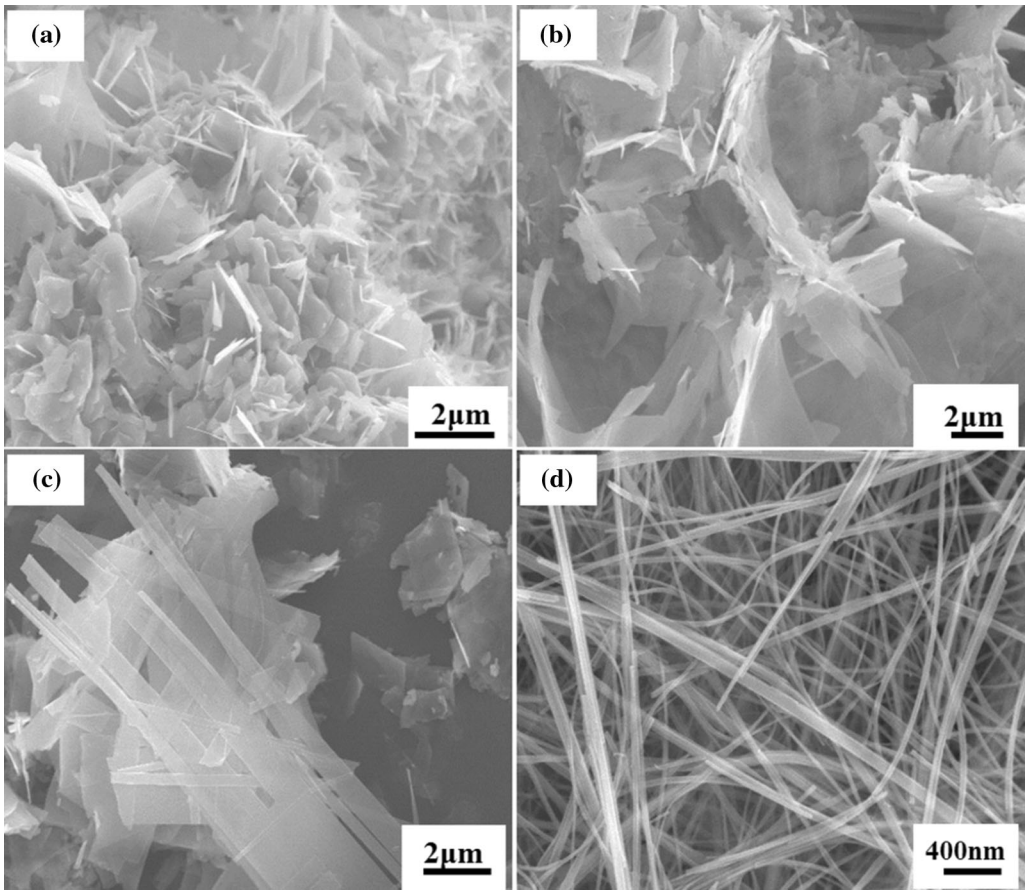

Fig. 2. SEM images of $LiMnO_2$ samples obtained at different time points during the reaction: (a) 24 h, (b) 48 h, (c) 72 h, and (d) 96 h.

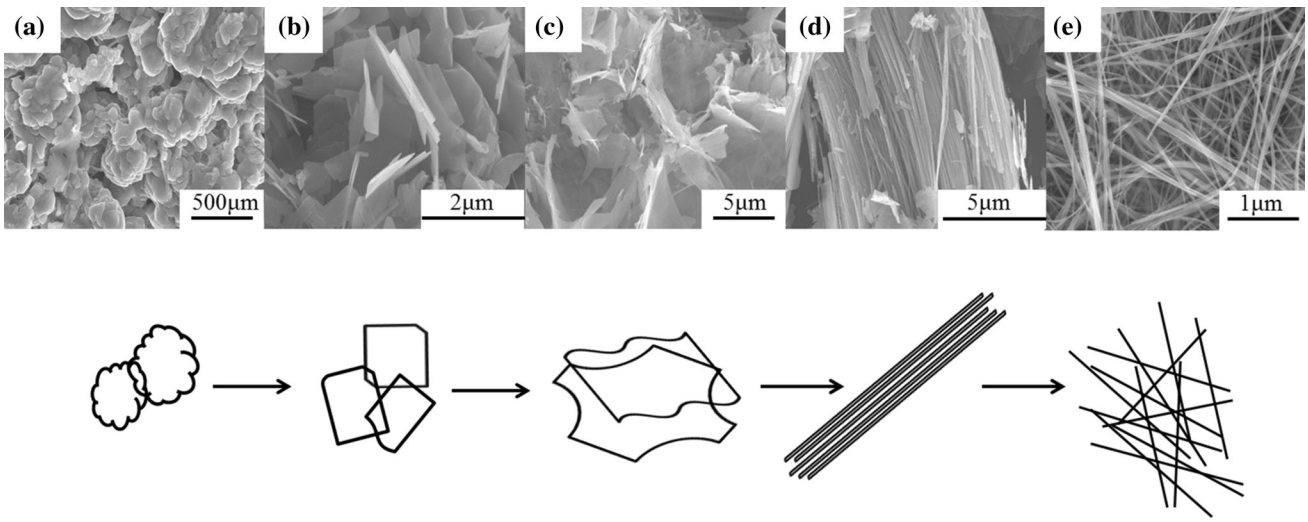

Fig. 3. Schematic illustration of the formation mechanism of the $LiMnO_2$ nanowires at different time points during the hydrothermal synthesis: (a) 0 h, bulk; (b) 24 h, plate; (c) 48 h, flake; (d) 72 h, bundle; (e) 96 h, nanowire.

In the working potential range of 0–0.5 V, the shapes of the CV curves correspond to a typical battery-like capacitive behavior that results from the faradaic redox reaction of Mn^{+3}/Mn^{+4} in the $LiMnO_2$ nanowires and $LiMnO_2$ nanowires-GNP composite during the charge and discharge processes.[24,25] The mechanism of the electrochemical reaction can be proposed based on a similar reaction[26]:

$$LiMnO_2 \underset{\text{Discharge}}{\overset{\text{Charge}}{\rightleftarrows}} LiMn_{1-x}O_2 + xMn^{4+} + xe^-$$

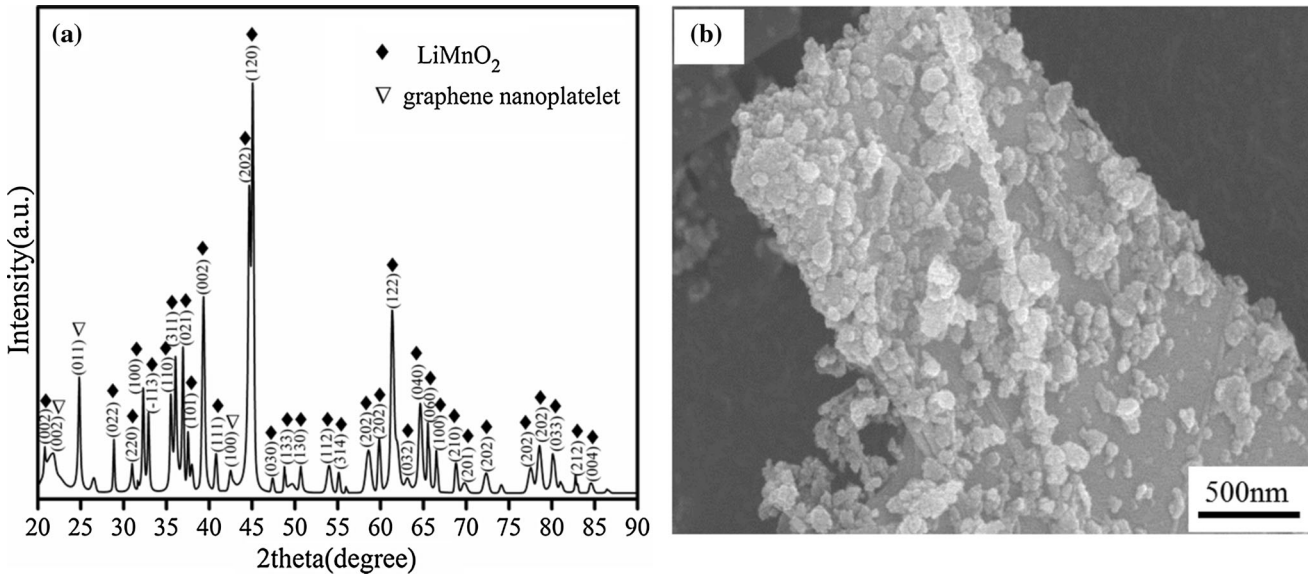

Fig. 4. (a) XRD pattern and (b) SEM image of $LiMnO_2$ nanowires-GNP composite.

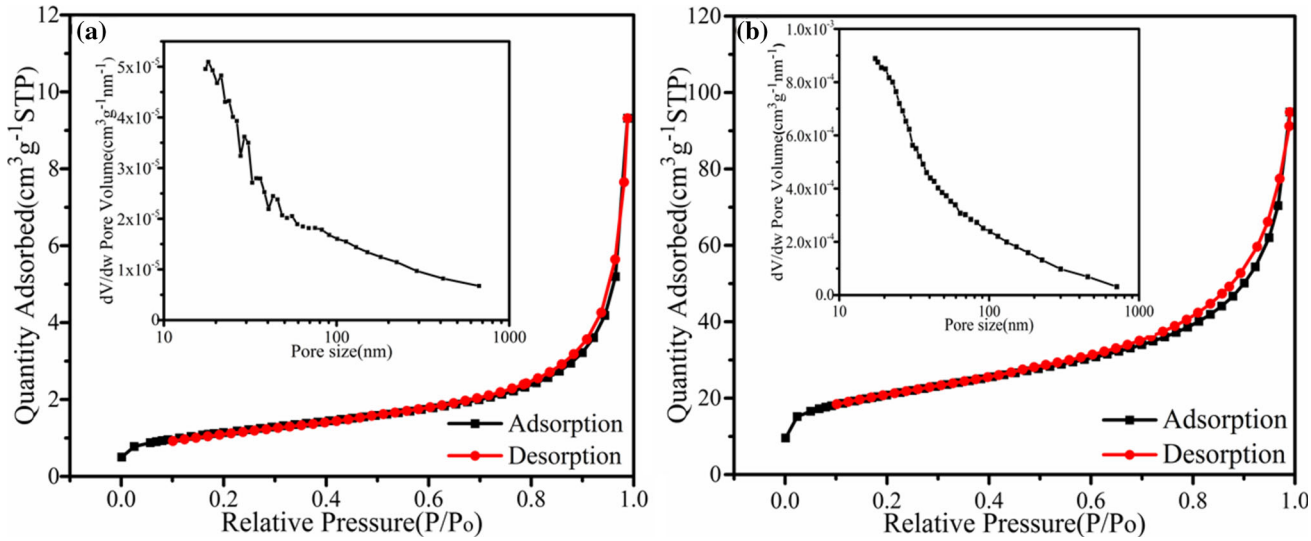

Fig. 5. N_2 adsorption–desorption isotherms and the corresponding pore size distribution (inset) of (a) $LiMnO_2$ nanowires and (b) $LiMnO_2$ nanowires-GNP composite.

The area under the CV curve is proportional to the charge stored during the anodic and cathodic scans. So, the CV curves were used to calculate the mass-specific capacitance. The plots of the mass-specific capacitance versus scan rates (in the range 5–100 mV s^{-1}) for both the electrodes materials are depicted in Fig. 6c. Similar to that observed in typical electrochemical capacitors, the specific capacitance of the $LiMnO_2$ nanowires and $LiMnO_2$ nanowires-GNP composite increased with decreasing scan rates. This is because of the limited diffusion of the electrolytes into the electrode materials, arising from the random distribution of pores on the surface of the electrodes.[27] The maximum mass-specific capacitance of $LiMnO_2$ nanowires-GNP composite obtained was as high as 147 F g^{-1} at 5 mV s^{-1}, which was more than three times higher than that of $LiMnO_2$ nanowires (41 F g^{-1}). The $LiMnO_2$ nanowires-GNP composite provides thorough access of the electrolyte ions to the electrode surface because of the good conductivity of graphene, leading to superior capacitance in comparison with the $LiMnO_2$ nanowires.[28] In order to further investigate the charging and discharging properties of $LiMnO_2$ nanowires and $LiMnO_2$ nanowires-GNP electrode materials, the galvanostatic charge–discharge characteristics were measured at a current density of 1 A g^{-1} in the potential range 0–0.5 V. The charge–discharge curves of the

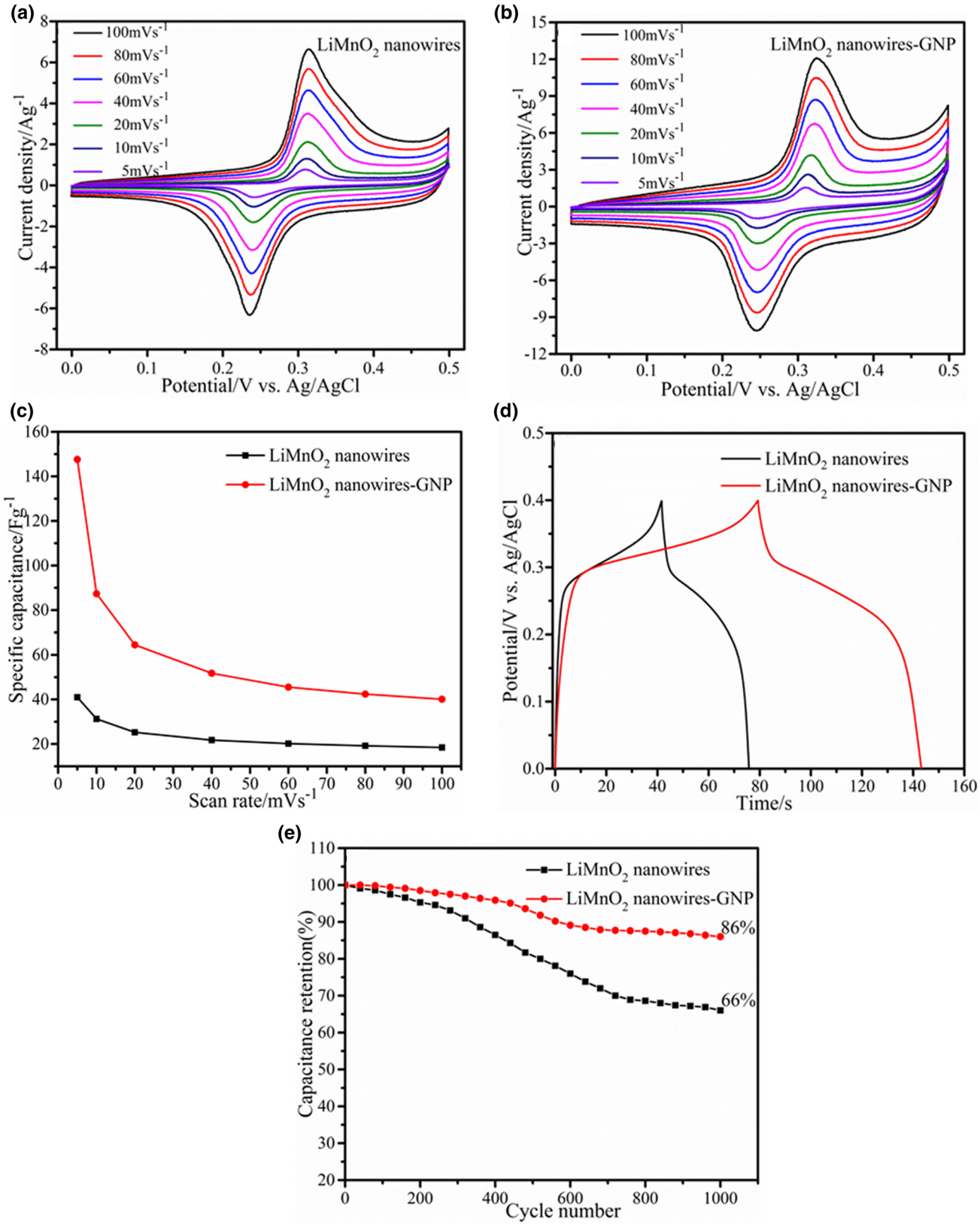

Fig. 6. Electrochemical characterizations of $LiMnO_2$ nanowires and $LiMnO_2$ nanowires-GNP composite as cathode materials in electrochemical capacitors: (a, b) CV curves of the two samples at various scan rates, from 5 mV s^{-1} to 100 mV s^{-1}, (c) variation in the mass-specific capacitance of the two CV curves as a function of the scan rate, (d) galvanostatic charge–discharge curves of $LiMnO_2$ nanowires and $LiMnO_2$ nanowires-GNP electrodes at a current density of 1 A g^{-1}, (e) cycling performances of the two electrode materials at a current density of 5 A g^{-1} for 1000 cycles.

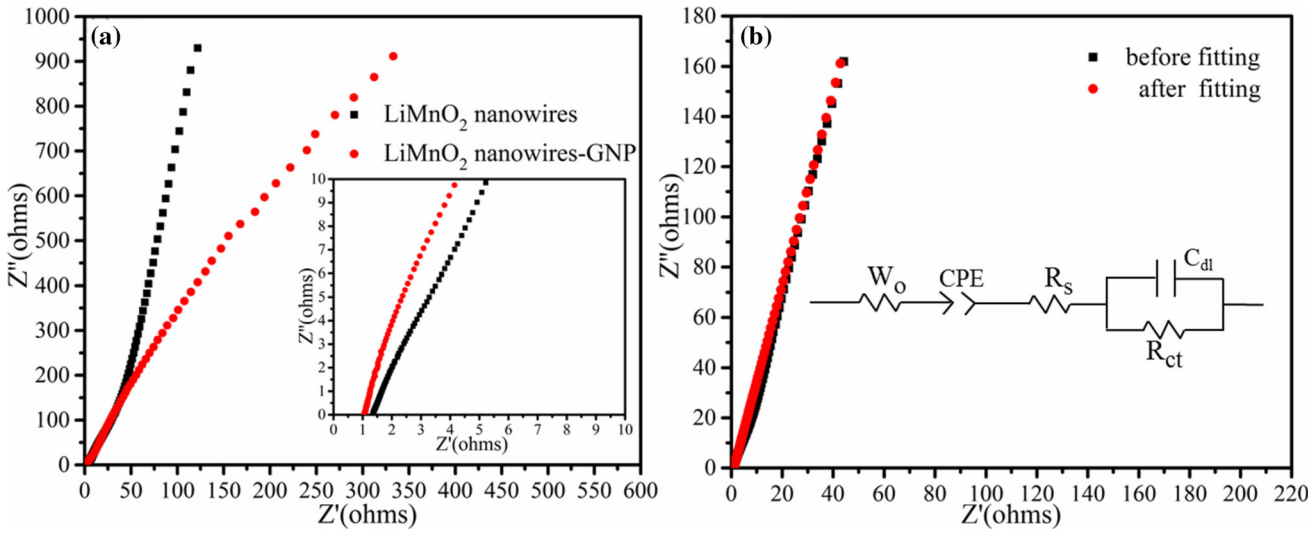

Fig. 7. (a) Nyquist plots of $LiMnO_2$ nanowires and $LiMnO_2$ nanowires-GNP composite as the cathode materials and (b) Nyquist plots of $LiMnO_2$ nanowires-GNP samples before and after fitting. Inset shows the fitted equivalent circuit: Wo, CPE, Rs, Cdl, and Rct refer to Warburg impedance, faradaic pseudocapacitance, series resistance, double layer capacitance, and faradaic charge transfer resistance, respectively.

electrodes presented in Fig. 6d are non-triangular, which are characteristic of pseudocapacitors. This also illustrates that the capacitive performance of the $LiMnO_2$ nanowires-GNP electrode material is more stable and reliable than that of $LiMnO_2$ nanowires. Moreover, the galvanostatic charge–discharge profiles are also used to calculate the capacitances using the formula $C_s = (I^*\Delta t)/(\Delta V^*m)$, where I, ΔV, Δt, and m represent discharge current, discharge time, potential window, and mass of the active materials, respectively. Using this equation, the specific capacitance of our $LiMnO_2$ nanowires-GNP electrode material was calculated to be 70 F g^{-1}. This value is within the capacitance range 43–147 F g^{-1}, calculated from the former CV curves, demonstrating that the capacitances calculated from the two curves agree with each other.

The cycling stability of the $LiMnO_2$ nanowires and $LiMnO_2$ nanowires-GNP composite electrodes were also examined from the galvanostatic charge–discharge profiles at a current density of 5 A g^{-1} for 1000 cycles. Figure 6e clearly shows that the capacitance retention of the $LiMnO_2$ nanowires-GNP is 86% after 1000 cycles, which is 20% higher than that of $LiMnO_2$ nanowires.

Finally, electrochemical impedance spectroscopy was performed to obtain further insights into the electrochemical properties of $LiMnO_2$ nanowires and $LiMnO_2$ nanowires-GNP electrode materials. From the x-axis intercepts of the Nyquist plots (Fig. 7a), the internal resistances of the $LiMnO_2$ nanowires-GNP electrode and $LiMnO_2$ nanowires electrode were calculated to be 1.03 Ω and 1.4 Ω, respectively.[5] This suggested that $LiMnO_2$ nanowires-GNP composite has lower interparticle resistance as compared with $LiMnO_2$ nanowires. Figure 7b shows the Nyquist plots of the $LiMnO_2$ nanowires-GNP electrode before and after fitting; the inset in Fig. 7b suggests a good fit of the Nyquist plot with the equivalent circuit.

CONCLUSIONS

In summary, well-dispersed one-dimensional $LiMnO_2$ nanowires of diameter of 100 nm were successfully prepared via a simple one-pot hydrothermal method. Based on the morphology transformation at different time points in the reaction, we proposed that the formation of $LiMnO_2$ nanowires followed a nucleation and regrowth process. The $LiMnO_2$ nanowires-GNP composite was then synthesized by the direct milling of one-dimensional $LiMnO_2$ nanowires and two-dimensional GNP. The $LiMnO_2$ nanowires-GNP composite exhibited an outstanding mass-specific capacitance of 147 F g^{-1} at 5 mV s^{-1}, as revealed by the cyclic voltammetry measurement. This was more than three times higher than that exhibited by $LiMnO_2$ nanowires (41 F g^{-1}). The cycling performance of $LiMnO_2$ nanowires-GNP electrode revealed a capacitance retention of 86% after 1000 charge–discharge cycles at 5 A g^{-1}, which was better than that exhibited by the $LiMnO_2$ nanowires. Besides, the resistance of the $LiMnO_2$ nanowires-GNP was lower than that of $LiMnO_2$ nanowires, demonstrating that these hybrids could be considered as next generation electrode materials for electrochemical energy storage and conversion devices.

ACKNOWLEDGMENTS

This research was supported by the Basic Science Research Program through the National Research Foundation of Korea (NRF) funded by the Ministry of Education (NRF-2017R1D1A1B03032466). This work was supported by the Technology Innovation Program (10052774, Development of hybrid super-

capacitor by nano structure carbon for ISG Applications) funded by the Ministry of Trade, Industry & Energy (MI, Korea).

CONFLICT OF INTEREST

The authors declare that they have no conflicts of interests.

REFERENCES

1. J.H. Bae, Y.J. Park, M.B. Lee, S.N. Cha, Y.J. Choi, C.S. Lee, J.M. Kim, and Z.L. Wang, *Adv. Mater.* 23, 3446 (2011).
2. S.C. Jun, W. Zhu, X.D. Wu, Q.F. Han, and X. Wang, *ACS Nano* 4, 2822 (2010).
3. J.H. Bae, M.K. Song, Y.J. Park, J.M. Kim, M.L. Liu, and Z.L. Wang, *Angew. Chem. Int. Ed.* 123, 1721 (2011).
4. J. Chow, R.J. Kopp, and P.R. Portney, *Science* 302, 1528 (2003).
5. X.L. He and J.H. Bae, *J. Electron. Mater.* 47, 5468 (2018).
6. M.J. Kim and J.H. Kim, *Electrochim. Acta* 260, 921 (2018).
7. M.M. Liu, J. Chang, Y. Bai, and J. Sun, *RSC Adv.* 5, 91389 (2015).
8. D.W. Wang, F. Li, and H.M. Cheng, *J. Power Source* 185, 1563 (2008).
9. P.G. Bruce, B. Scrosati, and J.M. Tarascon, *Angew. Chem. Int. Ed.* 47, 2930 (2011).
10. A.S. Arico, P.G. Bruce, B. Scrosati, J.M. Tarascon, and W. Schalkwijc, *Nat. Mater.* 4, 366 (2005).
11. Y. Kwon and J. Cho, *Chem. Commun.* 7, 1109 (2008).
12. M.G. Kim, M.K. Jo, Y.S. Hong, and J. Cho, *Chem. Commun.* 8, 218 (2009).
13. X. Li, F. Cheng, B. Guo, and J. Chen, *J. Phys. Chem. B* 109, 14017 (2005).
14. J.J. Niu, A. Kushima, X.F. Qian, and J. Li, *Nano Lett.* 14, 4005 (2014).
15. B.H. Zhang, Y. Liu, Z. Chang, Y.Q. Yang, Z.B. Wen, Y.P. Wu, and R. Holze, *J. Power Sources* 253, 98 (2014).
16. B.H. Zhang, Y. Liu, Z. Chang, Y.Q. Yang, Z.B. Wen, and Y.P. Wu, *Electrochim. Acta* 130, 693 (2014).
17. W.L. Cai, G.R. Li, K.L. Zhang, J.B. Zhou, Y.T. Qian, and J. Du, *Dalton Trans.* 45, 19221 (2016).
18. P. Xiong, J.W. Zhu, L.L. Zhang, and X. Wang, *Nanoscale Horiz.* 1, 340 (2016).
19. S. Bag and C.R. Raj, *J. Mater. Chem. A* 42, 17848 (2014).
20. M.J. Jing, C.W. Wang, H.S. Hou, X.N. Jia, Y. Zhang, and X.B. Ji, *J. Power Sources* 298, 241 (2015).
21. C.H. Wu, Q. Shen, R. Mi, S.X. Deng, Y.Q. Shu, H. Wang, and H. Yan, *J. Mater. Chem. A* 2, 15987 (2014).
22. A.K. Sinha, M. Pradhan, and T. Pal, *J. Phys. Chem. C* 117, 23976 (2013).
23. W.W. Sun, H.Q. Liu, Y.M. Liu, G.X. Bai, W.L. Shi, S. Guo, and X.Z. Zhao, *Nanoscale* 7, 13173 (2015).
24. Y. Gogotsi and R.M. Penner, *ACS Nano* 12, 2081 (2018).
25. H.Y. Liang, J.H. Lin, H.N. Jia, S.L. Chen, J.L. Qi, J. Cao, and T.S. Lin, *J. Power Sources* 378, 248 (2018).
26. Y.F. Yuan, K. Amine, J. Lu, and R.S. Yassar, *Nat. Commun.* 15806, 1 (2017).
27. Q.T. Qu, Y. Shi, S. Tian, Y.P. Wu, and R. Holze, *J. Power Sources* 194, 1222 (2009).
28. A. Pendashteh, S.E. Moosavifard, M.S. Rahmanifar, Y. Wang, R.B. Kaner, and M.F. Mousavi, *Chem. Mater.* 27, 3919 (2015).